JOURNAL OF MATERIALS SCIENCES **33** (1998) 2357–2363

Characterization of the damage process in short-fibre/thermoplastic composites by acoustic emission

N.S. CHOI
Department of Mechanical Engineering, Hanyang University, Ansan-si, Kyunggi-do 425-791 Korea

K. TAKAHASHI
Research Institute for Applied Mechanics, Kyushu University, Kasuga-shi, Fukuoka 816-8580 Japan
E-mail: k.takaha@riam.layvshu-u.ac.jp

Fracture processes of short glass fibre-reinforced thermoplastic tensile specimens have been investigated in relation to acoustic emission (AE) characteristics. Two fibre diameters ($d = 10$, 23 μm) were adopted for this study. Frequency analysis employing band-pass filters suggested that AE with higher amplitude was due to fibre breakages. Fibre–matrix interfacial failure and matrix fracture emitted lower amplitude AE waves. Reflected and transmitted optical microscopy, in combination with scanning electron microscopy, revealed that fibre breakage ahead of the artificial notch tip led to the initiation of a macroscopic fracture. This coincided with the results that AE peak amplitudes, V_p, showed a minimum at fracture initiation. When the macroscopic fracture propagated, V_p again increased rapidly, indicating additional fibre breakage. These fracture mechanism worked consistently for both $d = 10$ and 23 μm. Based on the above findings, AE source characterization was proposed for the stable fracture process of short fibre-reinforced plastics. © *1998 Chapman & Hall*

1. Introduction

Short fibre-reinforced plastics (SFRP) have been extensively utilized in industry as engineering materials. Their fracture behaviour has often been studied with the aid of acoustic emission (AE) techniques to obtain information valuable for improving their mechanical performance [1–5]. To make better use of the AE data obtained from SFRP, correlation with an individual fracture process in each material should be attempted; this is because the AE technique detects only stress waves which are generated during the transient dynamic fracture process although the fracture process is rather complex [6–8]. The present authors [9] recently measured quantitatively the effect of AE wave attenuation on the AE peak amplitude distribution and found that the peak amplitudes obtained from SFRP were considerably affected by attenuation during wave propagation in the specimen medium. It was also shown [10, 11] that AE characteristics were greatly affected by initial notch-tip radius which was influential in the damage initiation and fracture processes of SFRP specimens. The feature of AE peak amplitudes versus displacement coincided with the observed damage formation process. AE waves in a higher amplitude range corresponded to fibre breakage. Fibre breakage ahead of the notch tip was a prerequisite for the initiation of a main crack.

In this work, the influence of fibre diameter on AE characteristics of SFRP was studied in conjunction with fracture mechanisms. AE sources were proposed in relation to individual processes in the stable fracture of short fibre-reinforced plastics.

2. Experimental procedure

2.1. Specimens

Short glass fibre (SGF)-reinforced thermoplastic specimens were made from poly(ethylene terephthalate) (PET) and E-glass fibres. Fibres of different diameters (d = 10 and 23 μm) were treated with an amino-silane coupling and an epoxy sizing agent for good adhesion to the PET matrix. Tensile specimens were injection moulded and their dimensions were determined after ASTM D638. The gauge portion was 60 mm by 12.5 mm with a thickness of 3 mm. The mould fill direction (MFD) was the length direction of the specimens, as shown in Fig. 1. The fibre weight fraction was about 30%. Lengths of the 10 μm diameter fibres had a distribution with a peak at about 153 μm in the range 20–580 μm, while those of 23 μm diameter a distribution of 35–1160 μm with a peak at 280 μm. As exhibited in Fig. 2, the fibres became oriented mostly in the MFD. The PET resin was in an amorphous state. The gauge portion of the specimens was

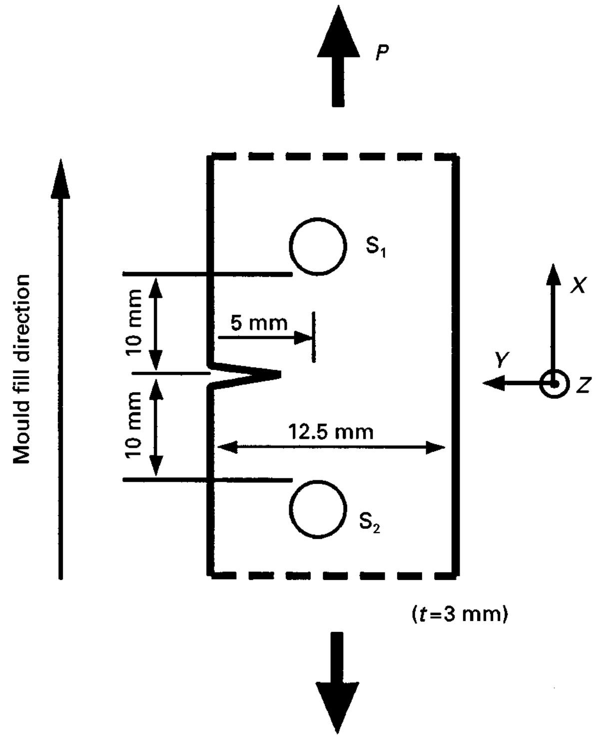

Figure 1 Notched specimen of injection-moulded SGF 30 wt % PET and AE sensor locations (S_1, S_2).

single-edge notched with a diamond cutter and a sharp notch was introduced by pushing a fresh razor blade into the initial notch tip. The notch depth was kept to 5.0 ± 0.2 mm (see Fig. 1).

2.2. Acoustic emission measurements

AE measurements were performed during the tensile test employing the Nippon Steel AE Inspection System (NAIS-AE5000). Five specimens were tested for each fibre diameter. AE waves were detected by two sensors (F217-M) having similar broad-band characteristics (50–700 kHz with peak sensitivity at 200 kHz). The sensors were set on the surface of the same side of the specimen using silicone grease under constant pressure (see S_1 and S_2 in Fig. 1). The distance between either of the sensors and the initial notch tip was kept to 10.0 ± 0.2 mm. Measurement conditions are listed in Table I. A microcomputer (AE5800) determined source locations of detected AE waves on the basis of time data of wave arrival at the sensors S_1 and S_2, and on a preset wave-velocity datum. Thus, it automatically eliminated noise from outside of the measured portion. Only the waves detected by one sensor were adopted as AE data (Ch. 2). The AE peak amplitudes were compensated for attenuation loss as stated elsewhere [9]. During the AE measurement, the frequency of the AE waves was analysed using three band-pass filters, F_i, with frequency ranges of 70–157 kHz (Ch. 3, L), 142–312 kHz (Ch. 4, M) and 273–596 kHz (Ch. 5, H) as illustrated in Fig. 3. These filters were connected to the preamplifier output and were operated in parallel.

2.3. Fractography

Fracture behaviour of the SFRP specimens were examined using a polarized optical microscope.

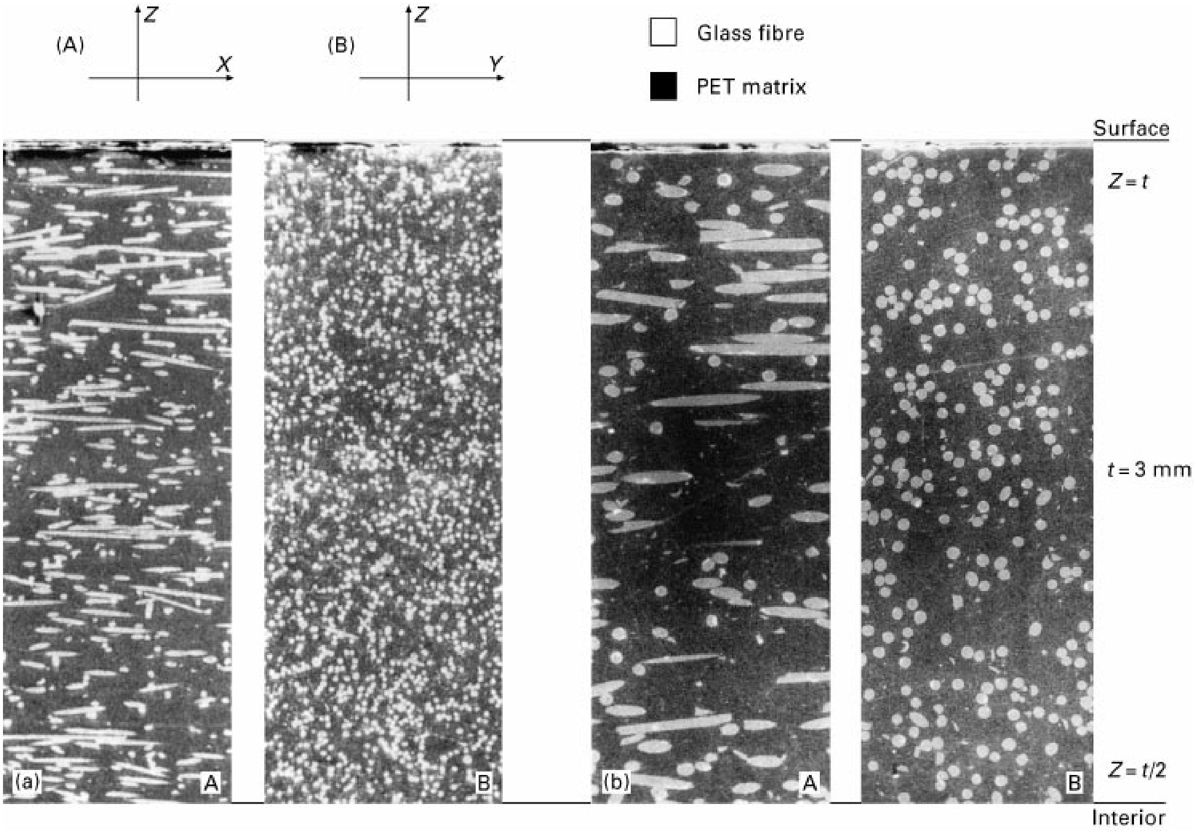

Figure 2 Orientation of short glass fibres embedded in thermoplastic matrix specimens for (a) $d = 10$ μm and (b) $d = 23$ μm (for coordinates, see Fig. 1).

TABLE I Measurement conditions

Specimen elongation rate	0.5 mm min^{-1}
Frequency band-pass	0–1.2 MHz
Pre-amp gain	40 dB
Main-amp gain	40 dB
Threshold level	0.25 V
Wave propagation velocity	2500 m s^{-1} [9–11]
Wave attenuation	0.18 dB mm^{-1} [9]

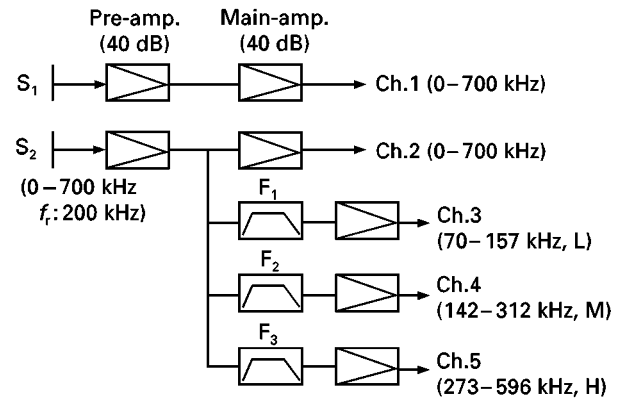

Figure 3 Band-pass filters, F_i, in connection with pre-amp output.

Specimens were thinned and polished to a thickness of about 80 μm employing a technique described earlier [12]. Reflected and transmitted light microscopy were utilized to study fracture morphology for the surface and interior of the thinned sections, respectively. As a complement to the optical microscopy, scanning electron microscopy (SEM) was utilized to observe fracture surfaces.

3. Results and discussion

3.1. Acoustic emission characteristics

Fig. 4 shows typical load P–displacement, δ, curves and accompanying changes of the cumulative AE event counts; ΣN, for SGF 30 wt % PET specimens. For each specimen, detectable AE events occurred at a displacement of 0.23 mm corresponding to about 35% of the maximum load, $P_{\max}$ and then ΣN increased slowly. With increasing δ, ΣN rapidly increased forming an exponential curve. However, the growth rate of ΣN slowed down at about 85% and 88% $P_{\max}$ for $d = 10$ and 23 μm, respectively. This abrupt change in the ΣN growth rate suggests that there was some significant change in the fracture process. With further loading up to the catastrophic fracture point, ΣN again greatly increased, showing an irregular growth rate. Compared with the results for $d = 10$ μm, specimens of $d = 23$ μm revealed lower average growth rate of ΣN, lower $P_{\max}$ and greater fracture displacement.

Fig. 5 shows histograms of AE peak amplitudes, V_p, against δ of the specimen of $d = 23$ μm in Fig. 4. The V_p in the figure is the average voltage, referring to the preamp input, of the peak amplitude for one event, which was obtained during each AE measurement time of 0.8 s. Because the upper bound for detectable V_p is 12.7 mV in this measurement, the average value

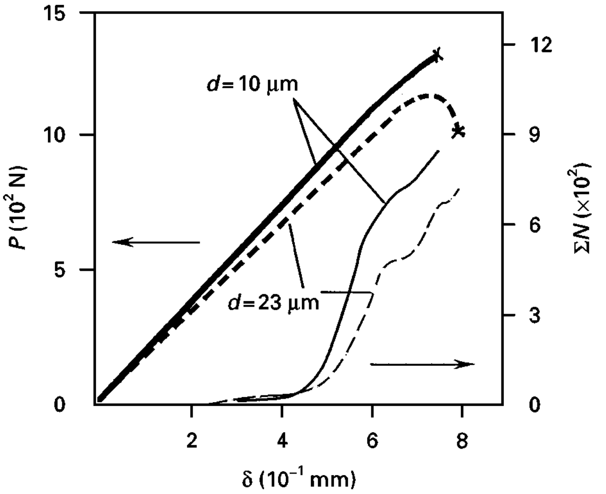

Figure 4 Typical curves of load, P, and AE events, ΣN, versus displacement, δ, for SGF 30 wt % PET specimens with fibres of different diameter, d.

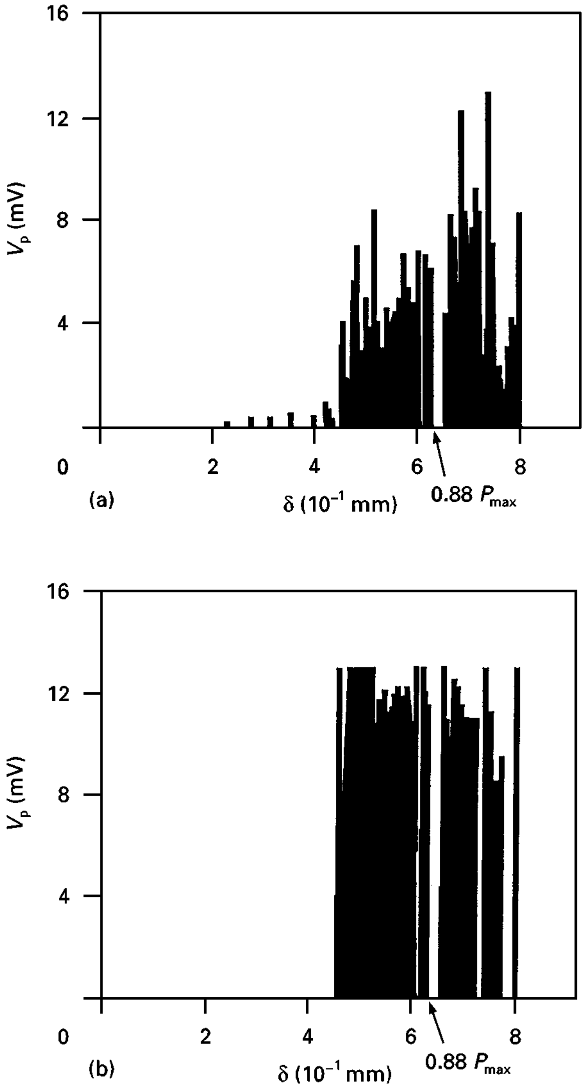

Figure 5 AE peak amplitude, V_p, versus displacement, δ, for the specimen with fibres of $d = 23$ μm in Fig. 4: (a) $V_p \geqslant 25$ μV, (b) $V_p \geqslant 7.0$ mV. Each value of V_p in the figure refers to the preamp input, which indicates average voltage of the peak amplitudes obtained for each measurement period of 0.8 s. The upper bound for detectable V_p is 12.7 mV.

must be much larger than that seen in Fig. 5. Results for V_p in a voltage range above the threshold voltage (V_{th}, 25 μV referring to the preamp input) are shown in Fig. 5a. With increasing δ, V_p first increased quickly up to a maximum and then decreased to a minimum or zero at $\delta = 0.65$ mm which corresponded to 88% P_{max}. At this time, the growth rate of ΣN lessened suddenly, as exhibited in Fig. 4. As δ increased further, V_p was again rapidly increased. Fig. 5b reveals the behaviour of V_p in a higher amplitude range above 7.0 mV. In the load stage where ΣN rapidly increased as shown in Fig.4, higher V_p was clearly apparent. It should be noted that all AE waves detected were a burst type and their duration was 50 μs–35 ms, which indicates that they were generated during dynamic and discontinuous microfracture processes in the specimen. It is believed that the feature of V_p is significantly associated with damage initiation and fracture process ahead of the notch tip.

The behaviour of V_p against δ for $d = 10$ μm shown in Fig. 6 was quite similar to that for $d = 23$ μm in Fig. 5, except that the value of the latter was on average 2.4 times larger than that for the former.

Values of V_p in Figs 5 and 6 were provided from AE signals taken by a sensor having a detectable range of 50–700 kHz with a resonant frequency of 200 kHz. Fig. 7a shows results of V_p for a specimen of $d = 23$ μm. The result of Ch. 2 in the figure is the same as that in Fig. 5a, while Ch. 3, Ch. 4 and Ch. 5 are results from the L, M and H band-pass devices, respectively. In the higher amplitude range beyond 7.0 mV, however, values of V_p were mostly from H band-pass and partly from M band-pass, which is distinctly indicated in Fig. 7b. Thus AE waves with higher amplitudes are related with higher frequency (H, M), whereas waves with lower amplitudes tend to involve a broad range of frequencies (L, M, H).

On the other hand, results of V_p for a specimen of $d = 10$ μm were also distributed all over the band-pass ranges [10, 11], which exhibited a feature consistent with those for $d = 23$ μm. This suggests that the fracture mechanisms generating AE waves were almost independent of d.

By studying the frequency spectrum of an AE signal taken from fracture of single glass fibre-embedded polycarbonate, Wolters [2] suggested that fibre fracture emitted lower and higher frequency waves, and that debonding and/or friction between fibres and matrix caused emission of waves of lower frequencies. Koenczoel *et al.* [4] employed notched specimens of short fibre/poly(vinyl chloride) composite and reported that the amplitude distribution of AE events became bimodal at crack speeds beyond 3 μm s^{-1}, and the higher and lower amplitudes were probably associated with fibre breakage and matrix fracture, respectively. Investigating glass fibre/epoxy SMC composite, on the other hand, Suzuki *et al.* [5] suggested that fibre breakage involved higher frequency waves of 250–400 kHz and that matrix cracking and fibre pull-out generated waves with a frequency range below 250 kHz. Results of the

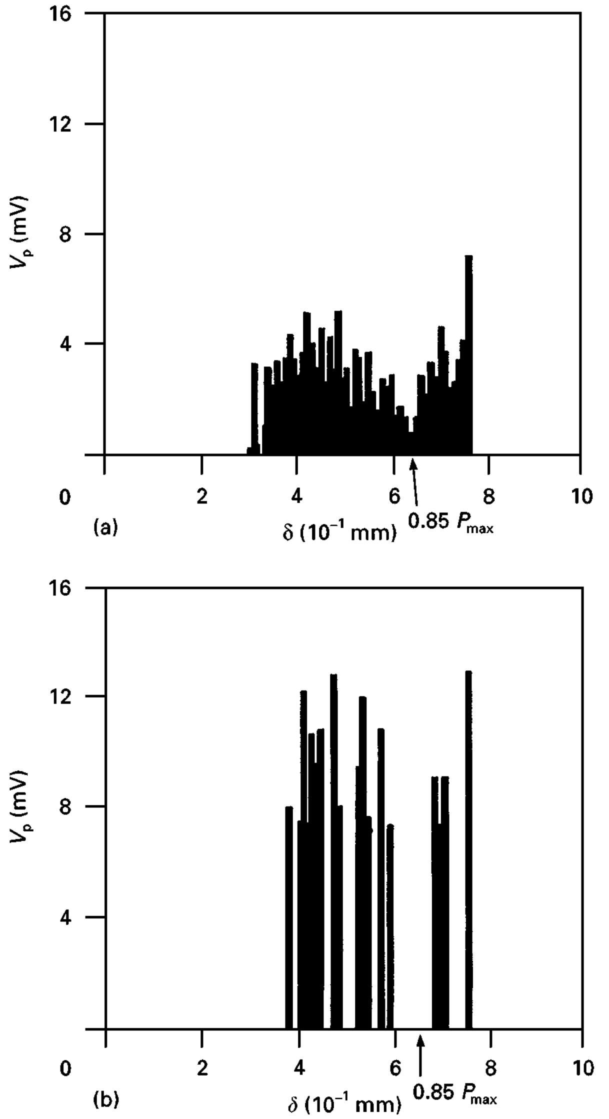

Figure 6 AE peak amplitudes, V_p, versus displacement, δ, for the specimen with fibres of $d = 10$ μm in Fig. 4: (a) $V_p \geqslant 25$ μV, (b) $V_p \geqslant 7.0$ mV. For the value of V_p, see caption to Fig. 5.

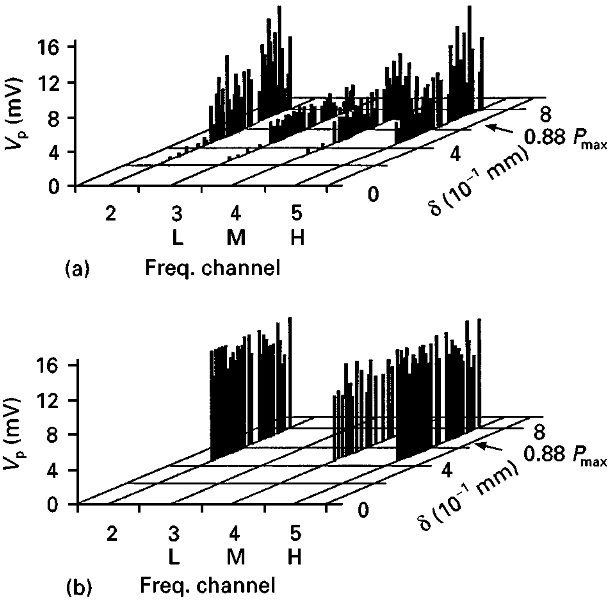

Figure 7 Frequency dependent V_p distribution for $d = 23$ μm in Fig. 5 (Ch. 2) classified by the band-pass filters (L, M, H): (a) $V_p \geqslant 25$ μV, (b) $V_p \geqslant 7.0$ mV. For the value of V_p at each channel, see caption to Fig. 5.

present investigation revealed that, first, all AE peak amplitudes could be classified according to frequency bands and secondly, the fracture processes generating AE waves were consistent for the specimens of different fibre diameters.

On the basis of the above findings on AE amplitude and frequency characteristics, as well as those of Wolters [2], Koenczoel *et al.* [4] and Suzuki *et al.* [5], it is believed that the higher amplitude waves are generated from fibre breakage and the lower amplitude waves from interfacial debonding or friction and matrix cracking.

3.2. Fracture mechanisms

Transient dynamic processes during damage initiation and growth in short fibre-reinforced thermoplastic composites generate AE waves. The above stated features of AE may be strongly associated with the individual fracture mechanism. Reflected and transmitted light microscopy in combination with scanning electron microscopy (SEM) were utilized to study further the fracture mechanisms.

Fig. 8 shows typical polarized optical micrographs taken from polished thin sections of a specimen of $d = 23$ μm. A section obtained from a specimen loaded up to about 88% $P_{\max}$ was observed under reflected light (Fig. 8a). Several voids were seen at the fibre ends in front of the notch tip. The merging of the voids seemed to cause the initiation of the main crack. When the same section was viewed under transmitted light (Fig. 8b), however, a damage zone was very obvious ahead of the notch tip with a size of about 940 μm in width and 1400 μm in length. It was ascertained that not only interfacial voiding but also fibre breakages and matrix failure were generated in the damage zone. Many of these microfailures joined together forming local failure facets in an approximately tensile mode.

Fig. 9a presents a polarized light micrograph taken in transmission through a thinned specimen of $d = 23$ μm sectioned perpendicular to the fracture surface. It is shown that the main crack propagated slowly about 2.4 mm from the notch tip just before catastrophic fracture. Fig. 9b and c shows scanning electron micrographs taken on the fracture surfaces located at A and B in Fig. 9a, respectively. Fibre pull-out from the matrix, as well as matrix plastic yielding and ductile separation, are shown on the stable fracture region. As seen by arrows in Fig. 9b, fibres were broken in a brittle manner, mostly towards the radial direction. Assuming that I_p is proportional to the created fracture surface area of the fibres, values of V_p for specimens of $d = 23$ μm should be approximately 5.3 times larger than those for $d = 10$ μm. This agreed with the results that values of V_p in a higher amplitude range for $d = 23$ μm (see Fig. 5b) were much larger than those for $d = 10$ μm (see Fig. 6b). If one assumes that the damage was initiated at the time of AE occurrence, the total time to create the stable fracture zone was calculated as about 72 s. The average growth rate of the zone was thus 33.3 μm s^{-1}.

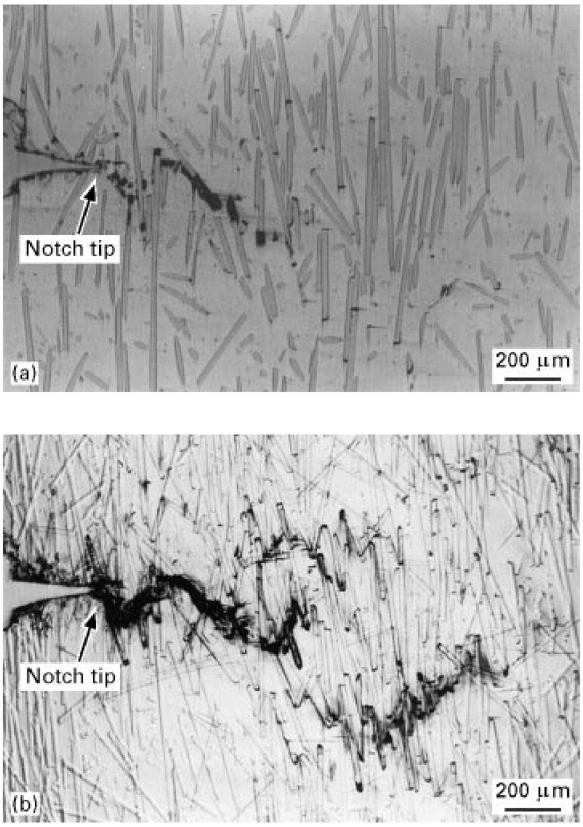

Figure 8 Polarized optical microscopy observation of fracture processes in the specimen with fibres of $d = 23$ μm. (a, b) Micrographs taken under reflected and transmitted light, respectively, from a thin section obtained after loading to about 88% maximum load. A damage zone, revealing fibre breakages and matrix microfailures, is clearly visible ahead of the notch tip in (b), whereas only macroscopic separation by joining together of voids can be seen in (a).

Fracture mechanisms for $d = 10$ μm observed in Fig. 10, in contrast, were quite analogous to those for $d = 23$ μm as described above, in that many fibre breakages (see Fig. 10b) occurred in advance of the main crack start (Fig. 10a) and the stable fracture proceeded with fibre breakage, fibre pull-out and matrix plastic separation.

3.3. Characteristic behaviour of AE sources

Possible AE sources during the fracture of SFRP are generally thought to be interfacial microcracking or debonding, matrix fracture, fibre pull-out and fibre breakage [1–5, 10, 11].On the basis of the above results from the fracture and AE studies, a model for the stable fracture process is schematically presented in Fig. 11. Fibre breakage emitted AE waves of higher amplitude, while interfacial and matrix fracture generated lower amplitude waves. The characteristic feature of V_p versus the displacement described in Figs 5 and 6 is of particular focus. The results for higher V_p suggest that fibre breakage played a significant role in the main crack initiation. Many local tensile fractures followed the pathways spanned by numerous reinforcing fibres. Many fibres were broken in front of the initial notch tip for both $d = 10$ and 23 μm (see Figs 8–10) and these are believed to have hindered the

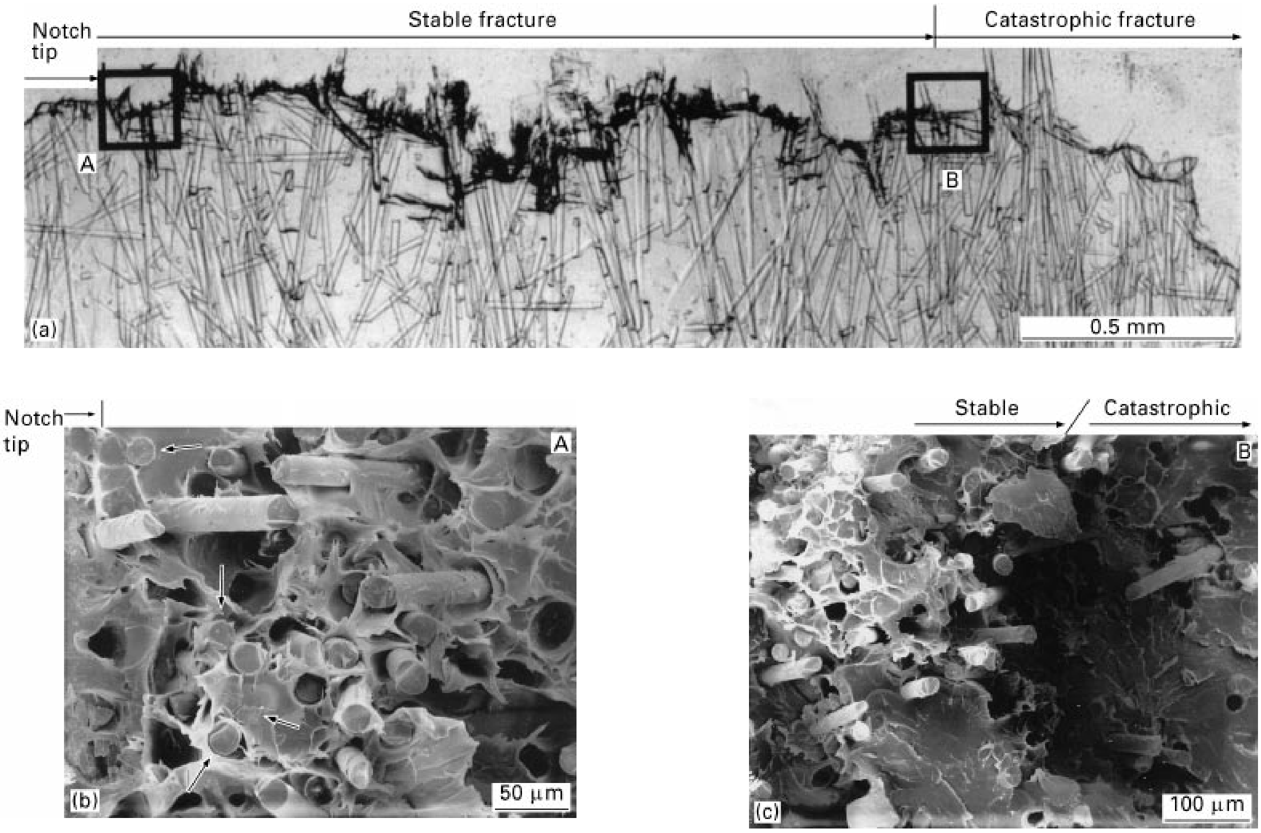

Figure 9 Observation of fracture surface of the specimen with fibres of $d = 23$ μm. (a) Polarized light in transmission from a thinned specimen sectioned vertical to the fracture surface. (b, c) SEM micrographs taken from areas A and B designated in (a). Fibre breakage, fibre pull-out and matrix ducitle separation were ascertained in the stable fracture zone.

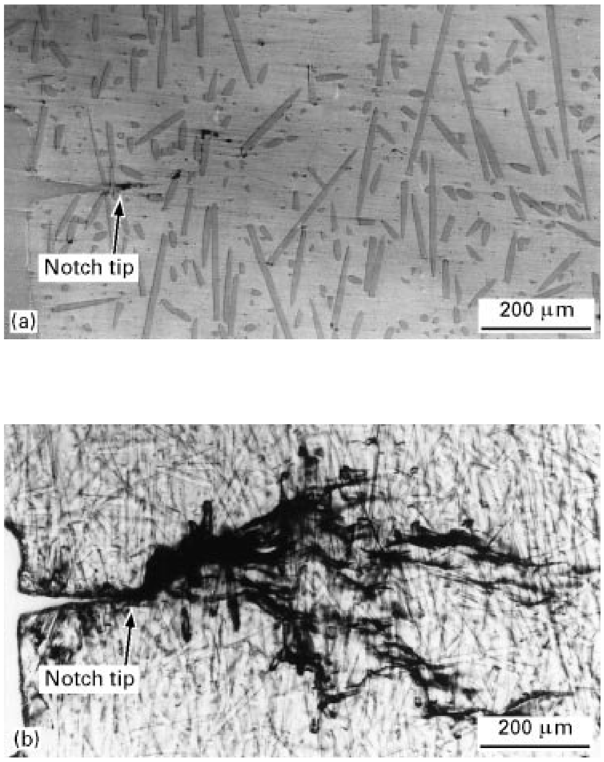

Figure 10 Polarized optical microscopy observation of fracture processes in the specimen with fibres of $d = 10$ μm. (a, b) Micrographs taken under reflected and transmitted light, respectively, from a thinned section obtained after loading to about 85% maximum load.

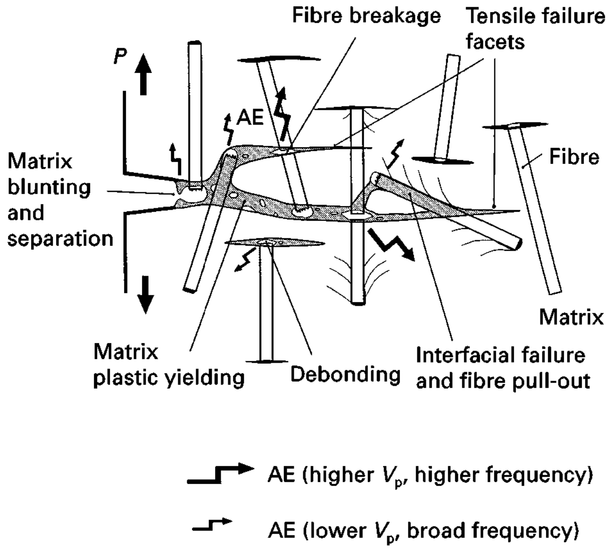

Figure 11 Schematic mechanism of AE sources in short fibre-reinforced plastics.

crack initiation [13, 14]. After the fibre breakage, the local failures grew to initiate a main crack. This clearly corresponded to the above AE results in that V_p in a higher amplitude range showed a minimum at the crack initiation, which is schematically shown in Fig. 12. During the propagation of the main crack, additional fibre breakages were induced depending on the extent of the damage zone.

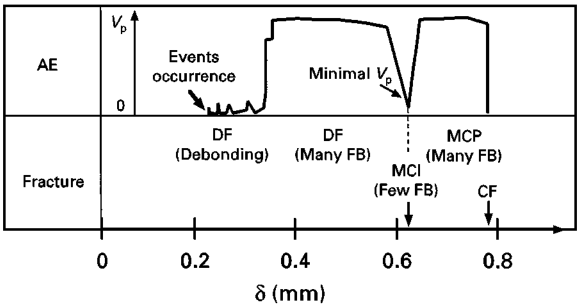

Figure 12 Characteristic behaviour of AE peak amplitudes describing the fracture process of short fibre-reinforced plastics. FB, fibre breakage; DF, damage formation; MCI, main crack initiation; CF, catastrophic fracture; MCP, main crack propagation.

4. Conclusions

Influence of fibre diameter ($d = 10$, 23 μm) on AE characteristics of SFRP has been investigated in relation to fracture mechanisms. The behaviour of AE peak amplitudes, V_p, versus displacement coincided with the observed fracture processes: V_p in a higher amplitude range exhibited a minimum at the initiation of the main crack. Frequency analysis utilizing band-pass filters suggested that AE events for the higher amplitude corresponded to fibre breakage. Interfacial failure and matrix fracture generated AE waves with lower amplitudes. Reflected and transmitted optical microscopy, in combination with scanning electron microscopy, revealed that fibre breakages ahead of the artificial notch tip played an important role in the initiation of a macroscopic fracture. These fracture mechanisms occurred consistently for both fibre diameters. Based on the observations, a model characteristic of AE occurrence in the stable fracture process has been proposed.

Acknowledgements

The authors are indebted to Nippon Steel Technos Co., which kindly provided the AE apparatus for this study. This work was supported by a Grant-in-Aid for Scientific Research from the Ministry of Education, Science, Sports and Culture of the Japanese Government, no. 07044160.

References

1. M. FAUDREE, E. BAER, A. HILTNER and J. COLLISTER, *J. Compos. Mater.* **22** (1988) 1170.
2. J. WOLTERS, in Proceedings of the 2nd International Symposium on Acoustic Emission from Reinforced Composites", Montreal (The Society of the Plastics Industry, Montreal, 1986) pp. 29–36.
3. N. SATO, T. KURAUCHI, S. SATO and O. KAMIGAITO, *J. Compos. Mater.* **22** (1988) 850.
4. L. KOENCZOEL, A. HILTNER and E. BAER, *Polym. Compos.* **8** (1987) 109.
5. M. SUZUKI, H. NAKANISHI, M. IWAMOTO, E. JINEN, Z. MAEKAWA and K. KOIKE, *J. Soc. Mater. Sci. Jpn* **36** (1987) 229 (in Japanese).
6. Y. H. PAO, R. R. GAJEWSKI and A. N. CERANOOGLU, *J. Acoust. Soc. Amer.* **65** (1979) 96.
7. K. TAKAHASHI, N. TAKEDA and T. HIGASHI, in "Proceedings of the 5th National Conference on Acoustic Emission" (The Japanese Society for Non-Destruction Inspection, Tokyo, 1985) pp. 7–12 (in Japanese).
8. M. A. HAMSTAD, *Exp. Mech.* **25** (1985) 7.
9. N. S. CHOI and K. TAKAHASHI, *J. Compos. Mater.* **24** (1990) 1012.
10. N. S. CHOI, K. TAKAHASHI and K. HOSHINO, in "Proceedings of the 11th International Acoustic Emission Symposium" (The Japanese Society for Non-Destruction Inspection, Tokyo, 1992) pp. 133–40.
11. N. S. CHOI, K. TAKAHASHI and K. HOSHINO, *NDTE Int.* **25** (1992) 271.
12. N. S. CHOI and K. TAKAHASHI, *J. Mater. Sci. Letter.* **12** (1993) 1718.
13. V. C. LI, Y. WANG and S. BACKER, *J. Mech. Phys. Solids* **39** (1991) 607.
14. N. S. CHOI and K. TAKAHASHI, *J. Mater. Sci.* **31** (1996) 731.

Received 24 March
and accepted 5 December 1997